Volume 54 | Number 100 | 28 December 2018 | Pages 14037–14154

ChemComm

Chemical Communications

rsc.li/chemcomm

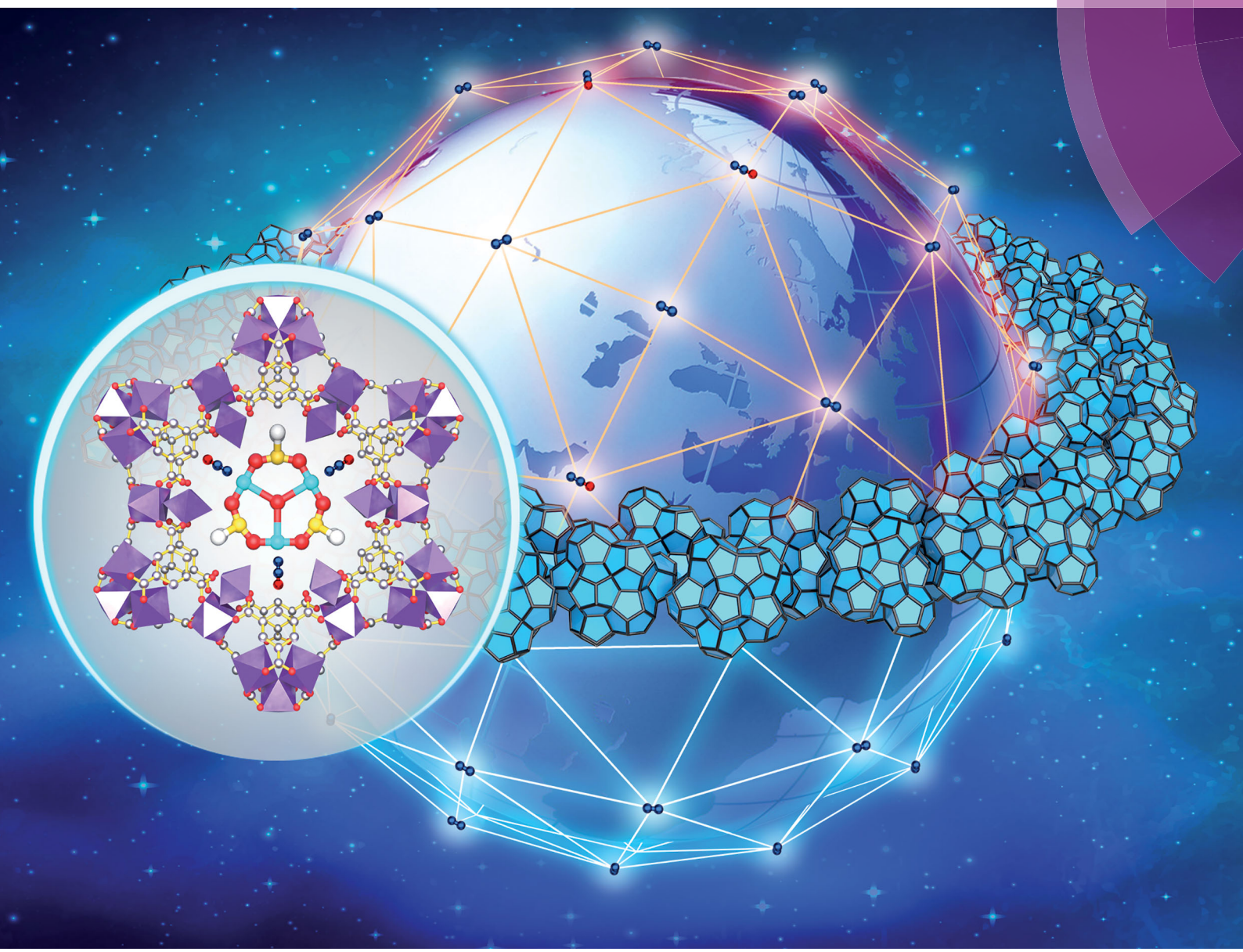

ISSN 1359-7345

ROYAL SOCIETY OF CHEMISTRY

COMMUNICATION

Jinping Li, Banglin Chen *et al.*

MIL-100Cr with open Cr sites for a record N_2O capture

ChemComm

COMMUNICATION

View Article Online
View Journal | View Issue

Cite this: *Chem. Commun.*, 2018, 54, 14061

Received 24th September 2018,
Accepted 12th November 2018

DOI: 10.1039/c8cc07679k

rsc.li/chemcomm

MIL-100Cr with open Cr sites for a record N_2O capture†

Jiangfeng Yang,[ab] Bingjie Du,[a] Jiaqi Liu,[a] Rajamani Krishna,[c] Feifei Zhang,[a] Wei Zhou,[d] Yong Wang,[b] Jinping Li*[ab] and Banglin Chen*[e]

Nitrous oxide (N_2O) is considered as the third most important greenhouse gas after carbon dioxide and methane and needs to be removed from air. Herein, we reported the metal–organic framework MIL-100Cr with open Cr sites for record N_2O capture capacities of 5.78 mmol g^{-1} at 298 K and 8.25 mmol g^{-1} at 273 K, respectively. DFT calculations showed that the static binding energy of N_2O on the open-Cr site is notably higher than that of N_2, 72.5 kJ mol^{-1} *vs.* 51.6 kJ mol^{-1}, which enforces MIL-100Cr to exhibit extremely high N_2O/N_2 ideal adsorbed solution theory (IAST) gas separation selectivity up to 1000.

Nitrous oxide (N_2O) is the third most potent greenhouse gas after CO_2 and CH_4, and is involved in the depletion of stratospheric ozone with a 300-fold greater warming potential than CO_2.[1–4] Over the past few decades, N_2O has drawn the attention of researchers in various fields because of its involvement in some key biological processes such as denitrification, usage as the anesthetic medicine and the potent oxidizer for the formation of transition-metal oxocations.[5–7] It has been reported that about 40% of total N_2O emissions come from human activities, which arise from agriculture, transportation and industrial activities.[8–11] Along with the understanding of N_2O emissions, the degradation of N_2O into N_2 and O_2 is one of the recent research hotspots.[12–16] However, the catalytic decomposition of N_2O typically occurs at high temperature and N_2O cannot be recovered as a valuable intermediate for the production of other fine chemicals.[17,18] Therefore, the development of an efficient and economic technology to capture or concentrate N_2O is very important. However, capturing the trace amounts of N_2O (150 ppm or 0.015%) from air is an enormous challenge.[19,20] Unlike other active NO_X ($X \geq 1$) gases, N_2O is quite inert and exhibits kinetic stability that is very difficult to activate under mild conditions.[7] Porous adsorbents for the adsorptive capture of N_2O are the economic and effective materials for such a purpose.[21–26]

Previously, various porous adsorbents such as zeolite silicalite-1, zeolite-5A and porous carbon materials have been examined for N_2O capture with the maximal N_2O adsorption capacity of 4.10 mmol g^{-1} on zeolite-5A.[22–24] The emergence of new porous materials termed as metal–organic frameworks (MOFs) has enabled us to reach record materials for the capture and storage of CO_2, NH_3, CH_4, O_2 and H_2, attributed to their diverse crystal structures, high surface areas, tunable pore sizes and functional sites.[27–34] However, the record N_2O adsorption volume on MOFs was only 2.81 mmol g^{-1} (Ni-MOF),[26] which is even lower than the one reported on zeolite-5A.

With more and more MOFs developed, some potentially useful porous materials such as ZIF-8/MAF-4, UiO-66, and MIL-101/100 with both high thermal and water stability have been realized.[35–46] Typically, MOFs were activated under gentle conditions of comparatively low temperature and vacuum to sustain the framework structures. In certain cases, for example, for the MIL-100/MIL-101 series, such gentle activation might not be able to remove all the solvent molecules, particularly those strongly bound terminal solvent molecules with metal sites, so their adsorption performance might still have not been optimized as well. Chang *et al.* found that MIL-100Cr can be regenerated after being activated under a higher vacuum of 1×10^{-8} bar and a higher temperature of 523 K, exhibiting excellent performance for N_2 capture from CH_4 and O_2, and thus for N_2/CH_4 and N_2/O_2 adsorption separation.[47] This motivated us to do more in-depth studies on the activation of MIL-100Cr. To our surprise, the suitably activated sample of MIL-100Cr at 523 K and 1×10^{-10} bar for 12 h

[a] *Research Institute of Special Chemicals, College of Chemistry and Chemical Engineering, Taiyuan University of Technology, Taiyuan 030024, Shanxi, China. E-mail: jpli211@hotmail.com*
[b] *Shanxi Key Laboratory of Gas Energy Efficient and Clean Utilization, Taiyuan 030024, Shanxi, P. R. China*
[c] *Van 't Hoff Institute for Molecular Sciences, University of Amsterdam, Science Park 904, 1098 XH Amsterdam, The Netherlands*
[d] *NIST Center for Neutron Research, National Institute of Standards and Technology, Gaithersburg, Maryland 20899-6102, USA*
[e] *Department of Chemistry, University of Texas at San Antonio, One UTSA Circle, San Antonio, Texas 78249-0698, USA. E-mail: banglin.chen@utsa.edu*

† Electronic supplementary information (ESI) available: Standard XRD pattern, adsorption isotherms of N_2 and H_2O on MIL-100Cr *etc.* See DOI: 10.1039/c8cc07679k

can take up N_2O of 5.78 mmol g^{-1} at 298 K and 8.25 mmol g^{-1} at 273 K, setting record N_2O capture capacities among the developed porous materials. The gas separation selectivity of N_2O/N_2 (0.015%/99.985%) is accordingly very high up to 1000 under ambient conditions.

MIL-100Cr was prepared in our lab *via* a literature reported method and with some modifications (details shown in the ESI†).[48] Before the gas sorption studies, the MIL-100Cr was activated at 373 K for 12 h until there is no free water molecule in the structure, and then further activated in the *in situ* activation station for another 12 h under ultra-high vacuum (1×10^{-10} bar) and high temperature (423–573 K). The activated samples were named MIL-100Cr-*X* (*X* = 150/200/250/−275/300) to indicate the different activation temperatures of 150, 200, 250, 275 and 300 °C, respectively. The sample in the powder form was characterized by X-ray diffraction (PXRD), X-ray photoelectron spectroscopy (XPS) and Brunauer–Emmett–Teller (BET) analysis.

As shown in TGA,[46] MIL-100Cr is very stable up to 523 K. PXRD patterns (Fig. S1, ESI†) demonstrate that MIL-100Cr-250 indeed shows a high crystalline feature. The N_2O adsorption isotherms recorded for the activated MIL-100Cr at 298 K are shown in Fig. 1. When the activated temperature increases, the activated samples increase their uptakes for N_2O in which MIL-100Cr-250 (activated at 523 K) has the highest adsorption capacity (5.78 mmol g^{-1}). Compared with those reported materials such as zeolite and porous carbon for N_2O capture, MIL-100Cr-250 also has the highest N_2O capture capacity (Table 1).[21–24] The increase from 1.95 mmol g^{-1} in MIL-100Cr-150 to 5.78 mmol g^{-1} in MIL-100Cr-250 is remarkable, although there is only about 20% increase of their N_2 uptakes at 77 K (Fig. S2, ESI†), as well as the increase in their corresponding BET surface area from 1764 $m^2 g^{-1}$ to 2118 $m^2 g^{-1}$. Apparently, the higher temperature activation has enabled us to further remove those highly bound solvent molecules (with the metal sites). In fact, water adsorption studies indicated that MIL-100Cr-250 takes up 41 mmol g^{-1} water, while MIL-100Cr-150 adsorbs 32 mmol g^{-1} water (Fig. S3, ESI†). Once the activation temperature further increases above 250 °C, the N_2O capture amounts of the samples MIL-100Cr-275 and MIL-100Cr-300 decrease to about 5.46 mmol g^{-1}, which might be attributed to the partial collapse of the framework.

Table 1 N_2O adsorption capacity on several porous materials

Sorbent	N_2O (mmol g^{-1})	Temperature (K)	Ref.
Porous carbon	2.50	298	21
Silicalite-1	1.75	298	22
Zeolite-4A	3.50	298	23
Zeolite-5A	4.10	298	24
MOF-5	0.90	298	24
ZIF-7	2.50	298	25
Ni-MOF	2.81	298	26
MIL-100Cr-150	1.95	298	This work
MIL-100Cr-250	5.78	298	This work
MIL-100Cr-250	8.25	273	This work

As established before, there exists 2/3 terminal bound H_2O and 1/3OH^-/F^- sites which are distributed on the metal sites in MIL-100.[38–42] These terminal bound water molecules can be further removed at a very high temperature of 523 K and under vacuum below 1×10^{-8} bar to generate open Cr^{3+} sites (Fig. S4, ESI†) for the possible binding of N_2O molecules.[49] We believe that these open Cr^{3+} sites play a crucial role in the significant increase of N_2O uptakes from 1.95 mmol g^{-1} in MIL-100Cr-150 to 5.78 mmol g^{-1} in MIL-100Cr-250.

We calculated the isosteric heat of adsorption (Q_{st}) of N_2O in MIL-100Cr-250 bases on the adsorption isotherms (Fig. S5, ESI†) at 273 K and 298 K. As shown in Fig. S6 (ESI†), the Q_{st} of N_2O at low coverage is up to 80 kJ mol^{-1}, much higher than the Q_{st} of N_2 (39 kJ mol^{-1} [47]). Consistent with this, our DFT calculations (see the ESI† for details) also indicate that the static binding energy of N_2O at the open-Cr site is notably higher than that of N_2, 72.5 kJ mol^{-1} *vs.* 51.6 kJ mol^{-1} (the N_2 value being similar to the previously reported result, ~48.7 kJ mol^{-1} [47]). N_2O binds to the open-Cr through N, with a Cr–N bond distance slightly smaller than that found in N_2 binding (see Fig. 2).

We further used the adsorption selectivity used in the ideal adsorbed solution theory (IAST) to examine MIL-100Cr-250 to assess trace N_2O (150 ppm) separation from N_2 performance. The N_2 adsorption isotherms are shown in Fig. S7 (ESI†).

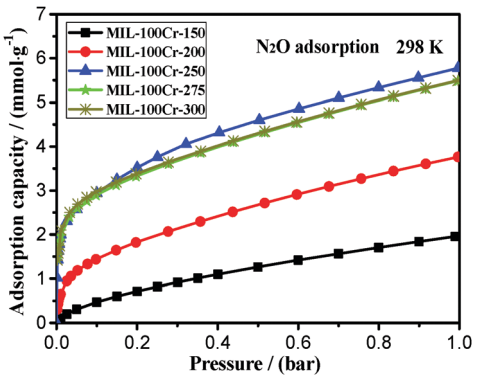

Fig. 1 Adsorption isotherms of N_2O at 298 K on MIL-100Cr activated at 423, 473, 523, 548 and 573 K.

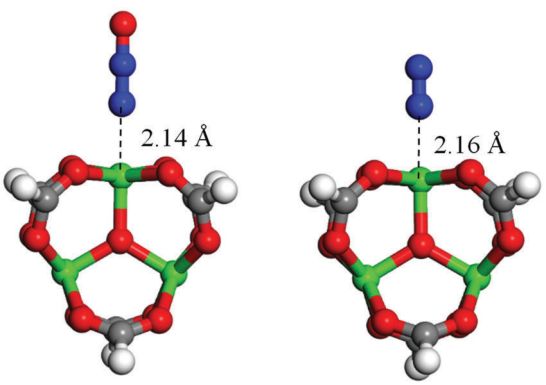

Fig. 2 The DFT-calculated adsorption configurations of N_2O and N_2 on the open-Cr sites in MIL-100Cr, using a cluster model. (Chromium, oxygen, nitrogen, carbon, and hydrogen atoms are in green, red, blue, gray and white, respectively.)

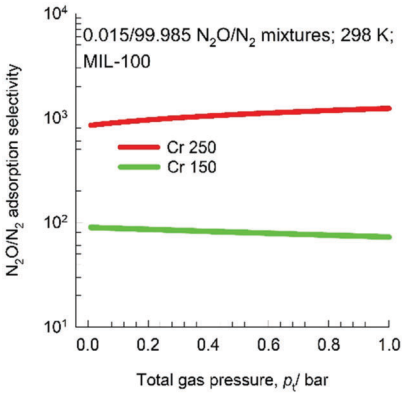

Fig. 3 Comparison of the ideal adsorbed solution theory (IAST) gas selectivity of 0.015/98.985 N_2O/N_2 mixtures in MIL-100Cr-150 and MIL-100Cr-250 at 298 K.

The N_2O and N_2 adsorption isotherm data were fitted with the dual-site Langmuir and single-site Langmuir models, respectively. Compared with MIL-100Cr-250 for its high N_2 selectivity from O_2 and CH_4,[46] the gas separation selectivity of N_2O from N_2 (N_2O/N_2 = 0.015/99.985) on MIL-100Cr-250 is significantly higher up to 1000 (Fig. 3). This is remarkable, indicating that trace amount of N_2O can be readily removed through a column packed with MIL-100Cr-250. As expected, MIL-100Cr-250 has much higher gas separation selectivities than MIL-100Cr-150 (about 100) as well. As shown in Fig. 4, simulated breakthrough curves further confirmed the significantly improved performance of MIL-100Cr-250 for this separation. The sorption data of CO_2, O_2 and CH_4 and possible separation of N_2O/CO_2, N_2O/O_2 and N_2O/CH_4 are provided in the ESI† (Fig. S8–S13).

In conclusion, through the optimized activation of the well-known, highly stable MIL-100Cr, we realized MIL-100Cr-250 as the best material for N_2O capture under ambient conditions with the capture capacity of 5.78 mmol g^{-1} at 298 K. Based on DFT calculations, the open Cr^{3+} sites are speculated to play crucial roles for the binding of N_2O with a binding energy of 80 kJ mol^{-1}. The promise of MIL-100Cr-250 for the removal of trace amounts of N_2O from N_2 was further evaluated *via* IAST studies, in which the gas separation selectivities of N_2O from N_2 on MIL-100Cr-250 are found to be the highest ones ever reported, up to 1000 and 100 times higher than those on MIL-100Cr-150. Given the fact that this MOF is highly stable, it might facilitate its practical use for this very important application. This work will also motivate us to explore more extensively those well-established MOFs to optimize their activation conditions and thus to maximize their multifunctional performances, particularly for gas storage and separation.

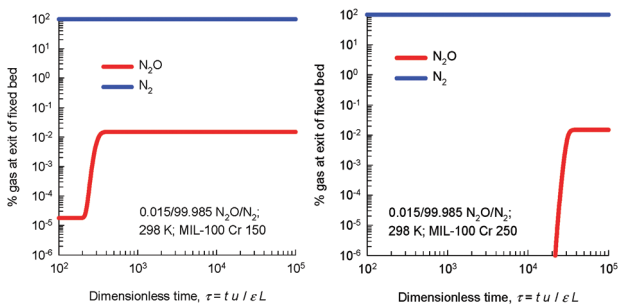

Fig. 4 Transient breakthrough simulation of 0.015/98.985 N_2O/N_2 mixtures in a fixed bed packed with MIL-100Cr-150 (left) and MIL-100Cr-250 (right) at 298 K and a total pressure of 1 bar.

This work was funded by the National Natural Science Foundation of China (No. 21676175 and 51672186) and partly by Welch Foundation (AX-1730).

Conflicts of interest

There are no conflicts to declare.

References

1 D. A. Lashof and D. R. Ahuja, *Nature*, 1990, **344**, 529.
2 J. T. Houghton, B. A. Callander and S. K. Varney, *Climate Change*, Cambridge University Press, 1992.
3 D. J. Wuebbles, *Science*, 2009, **326**, 56–57.
4 A. R. Ravishankara, J. S. Daniel and R. W. Portmann, *Science*, 2009, **326**, 123–125.
5 D. J. Xiao, E. D. Bloch, J. A. Mason, W. L. Queen, M. R. Hudson, N. Planas, J. Borycz, A. L. Dzubak, P. Verma, K. Lee, F. Bonino, V. Crocellà, J. Yano, S. Bordiga, D. G. Truhlar, L. Gagliardi, C. M. Brown and J. R. Long, *Nat. Chem.*, 2014, **6**, 590.
6 M. Konsolakis, *ACS Catal.*, 2015, **5**, 6397–6421.
7 K. Severin, *Chem. Soc. Rev.*, 2015, **44**, 6375–6386.
8 B. Anderson, K. Bartlett, S. Frolking, K. Hayhoe, J. Jenkins and W. Salas, Office of Atmospheric Programs, US EPA, EPA 430-R-10-001, Washington DC, 2010.
9 R. Reiner and S. Rudolf, *J. Plant Nutr. Soil Sci.*, 2015, **178**, 171–188.
10 A. Jurado, A. V. Borges and S. Brouyère, *Sci. Total Environ*, 2017, **584–585**, 207–218.
11 M. Jablonska and R. Palkovits, *Catal. Sci. Technol.*, 2016, **6**, 7671–7687.
12 K. Sun, H. Zhang, H. Xia, Y. Lian, Y. Li, Z. Feng, P. Ying and C. Li, *Chem. Commun.*, 2004, 2480–2481.
13 W. B. Tolman, *Angew. Chem., Int. Ed.*, 2010, **49**, 1018–1024.
14 S. M. Hamilton, W. S. Hopkins, D. J. Harding, T. R. Walsh, P. Gruene, M. Haertelt, A. Fielicke, G. Meijer and S. R. Mackenzie, *J. Am. Chem. Soc.*, 2010, **132**, 1448–1449.
15 M.-L. Tsai, R. G. Hadt, P. Vanelderen, B. F. Sels, R. A. Schoonheydt and E. I. Solomon, *J. Am. Chem. Soc.*, 2014, **136**, 3522–3529.
16 R. Zeng, M. Feller, Y. Diskin-Posner, L. J. W. Shimon, Y. Ben-David and D. Milstein, *J. Am. Chem. Soc.*, 2018, **140**, 7061–7064.
17 J. Pérez-Ramírez and M. Santiago, *Chem. Commun.*, 2007, 619–621.
18 N. J. Hartmann, G. Wu and T. W. Hayton, *Chem. Sci.*, 2018, **9**, 6580–6588.
19 X. Yang, A. Chen, J. Xie, T. Ding, W. Song, W. Lin and Y. Xie, *Proceeding of International Symposium on Eco Topia Science*, 2007.
20 R. N. van den Heuvel, M. M. Hefting, N. C. G. Tan, M. S. M. Jetten and J. T. A. Verhoeven, *Sci. Total Environ*, 2009, **407**, 2325–2332.
21 D. Saha and S. Deng, *J. Colloid Interface Sci.*, 2010, **345**, 402–409.
22 J. C. Groen, J. Pérez-Ramírez and W. Zhu, *J. Chem. Eng. Data*, 2002, **47**, 587–589.
23 D. Saha and S. Deng, *J. Chem. Eng. Data*, 2010, **55**, 3312–3317.
24 D. Saha, Z. Bao, F. Jia and S. Deng, *Environ. Sci. Technol.*, 2010, **44**, 1820–1826.
25 D.-L. Chen, N. Wang, F.-F. Wang, J. Xie, Y. Zhong, W. Zhu, J. K. Johnson and R. Krishna, *J. Phys. Chem. C*, 2014, **118**, 17831–17837.
26 X. Zhang, W. Chen, W. Shi and P. Cheng, *J. Mater. Chem. A*, 2016, **4**, 16198–16204.
27 A. R. Millward and O. M. Yaghi, *J. Am. Chem. Soc.*, 2005, **127**, 17998–17999.
28 B. Zheng, H. Wang, Z. Wang, N. Ozaki, C. Hang, X. Luo, L. Huang, W. Zeng, M. Yang and J. Duan, *Chem. Commun.*, 2016, **52**, 12988–12991.
29 F. Moreau, I. da Silva, N. H. Al Smail, T. L. Easun, M. Savage, H. G. W. Godfrey, S. F. Parker, P. Manuel, S. Yang and M. Schröder, *Nat. Commun.*, 2017, **8**, 14085.

30 B. Zheng, X. Luo, Z. Wang, S. Zhang, R. Yun, L. Huang, W. Zeng and W. Liu, *Inorg. Chem. Front.*, 2018, **5**, 2355–2363.
31 A. J. Rieth and M. Dincă, *J. Am. Chem. Soc.*, 2018, **140**, 3461–3466.
32 J. Jiang, H. Furukawa, Y.-B. Zhang and O. M. Yaghi, *J. Am. Chem. Soc.*, 2016, **138**, 10244–10251.
33 L. J. Murray, M. Dinca, J. Yano, S. Chavan, S. Bordiga, C. M. Brown and J. R. Long, *J. Am. Chem. Soc.*, 2010, **132**, 7856–7857.
34 B. Chen, N. W. Ockwig, A. R. Millward, D. S. Contreras and O. M. Yaghi, *Angew. Chem., Int. Ed.*, 2005, **44**, 4745–4749.
35 J. H. Cavka, S. Jakobsen, U. Olsbye, N. Guillou, C. Lamberti, S. Bordiga and K. P. Lillerud, *J. Am. Chem. Soc.*, 2008, **130**, 13850–13851.
36 M. Kandiah, M. H. Nilsen, S. Usseglio, S. Jakobsen, U. Olsbye, M. Tilset, C. Larabi, E. A. Quadrelli, F. Bonino and K. P. Lillerud, *Chem. Mater.*, 2010, **22**, 6632–6640.
37 R. Banerjee, A. Phan, B. Wang, C. Knobler, H. Furukawa, M. O'Keeffe and O. M. Yaghi, *Science*, 2008, **319**, 939–943.
38 X. C. Huang, Y. Y. Lin, J. P. Zhang and X. M. Chen, *Angew. Chem., Int. Ed.*, 2006, **45**, 1557–1559.
39 G. Ferey, C. Mellot-Draznieks, C. Serre, F. Millange, J. Dutour, S. Surble and I. Margiolaki, *Science*, 2005, **309**, 2040–2042.
40 P. Horcajada, S. Surble, C. Serre, D.-Y. Hong, Y.-K. Seo, J.-S. Chang, J.-M. Greneche, I. Margiolaki and G. Ferey, *Chem. Commun.*, 2007, 2820–2822.
41 C. Volkringer, D. Popov, T. Loiseau, G. R. Ferey, M. Burghammer, C. Riekel, M. Haouas and F. Taulelle, *Chem. Mater.*, 2009, **21**, 5695–5697.
42 A. Lieb, H. Leclerc, T. Devic, C. Serre, I. Margiolaki, F. Mahjoubi, J. S. Lee, A. Vimont, M. Daturi and J.-S. Chang, *Microporous Mesoporous Mater.*, 2012, **157**, 18–23.
43 J. Yang, J. Wang, S. Deng and J. Li, *Chem. Commun.*, 2016, **52**, 725–728.
44 H. Reinsch and N. Stock, *CrystEngComm*, 2013, **15**, 544–550.
45 D. F. Sava Gallis, K. W. Chapman, M. A. Rodriguez, J. A. Greathouse, M. V. Parkes and T. M. Nenoff, *Chem. Mater.*, 2016, **28**, 3327–3336.
46 G. Férey, C. Serre, C. Mellot-Draznieks, F. Millange, S. Surblé, J. Dutour and I. Margiolaki, *Angew. Chem., Int. Ed.*, 2004, **43**, 6296–6301.
47 J. W. Yoon, H. Chang, S.-J. Lee, Y. K. Hwang, D.-Y. Hong, S.-K. Lee, J. S. Lee, S. Jang, T.-U. Yoon, K. Kwac, Y. Jung, R. S. Pillai, F. Faucher, A. Vimont, M. Daturi, G. Férey, C. Serre, G. Maurin, Y.-S. Bae and J.-S. Chang, *Nat. Mater.*, 2016, **16**, 526.
48 P. Long, H. Wu, Q. Zhao, Y. Wang, J. Dong and J. Li, *Microporous Mesoporous Mater.*, 2011, **142**, 489–493.
49 J. W. Yoon, Y. K. Seo, Y. K. Hwang, J. S. Chang, H. Leclerc, S. Wuttke, P. Bazin, A. Vimont, M. Daturi, E. Bloch, P. L. Llewellyn, C. Serre, P. Horcajada, J. M. Greneche, A. E. Rodrigues and G. Ferey, *Angew. Chem., Int. Ed.*, 2010, **49**, 5949–5952.

MIL-100Cr with open Cr sites for a record N_2O capture

Jiangfeng yang[ad], Bingjie Du[a], Jiaqi Liu[a], Rajamani Krishna[b], Feifei Zhang[a], Wei Zhou[c], Yong Wang[d], Jinping Li[ad]*, Banglin Chen[e]*

[a] Research Institute of Special Chemicals, College of Chemistry and Chemical Engineering, Taiyuan University of Technology, Taiyuan 030024, Shanxi, P. R. China.

[b] Van 't Hoff Institute for Molecular Sciences, University of Amsterdam, Science Park 904,1098 XH Amsterdam, The Netherlands

[c] NIST Center for Neutron Research, National Institute of Standards and Technology, Gaithersburg, Maryland 20899-6102, United States.

[d] Shanxi Key Laboratory of Gas Energy Efficient and Clean Utilization, Taiyuan 030024, Shanxi, P. R. China.

[e] Department of Chemistry, University of Texas at San Antonio, One UTSA Circle, San Antonio, Texas 78249-0698, United States

Supporting Information

1. Experimental

1.1. Materials

MIL-100Cr was synthesized and purified according to the literature. [1] Mixed metallic chromium (0.104 g), H_3BTC (0.3 g), HF (40%, 0.2 mL) and deionized water (9.6 mL) evenly. The slurry was introduced in a 23 mL Teflon liner, which was then put into an oven. The system was heated from room temperature up to 493 K in 12h, and keep at 493 K for 4 days before being cooled to room temperature in 24 h. The resulting light green product was filtered off, immersed in ethanol at 343 K for 5 h at a ratio of 1 g / 250 mL to remove the excess of unreacted organic ligand and then filtered again. The solid was finally dried for 3 h in vacuum at 323 K. The resulting solid material was denoted as MIL-100Cr. MIL-101Cr was synthesized in our laboratory too. [2]

1.2. Characterization

The crystallinity and phase purity of the materials were measured by powder X-ray diffraction (PXRD) on a Bruker D8 ADVANCE X-ray diffractometer with Cu-Kα (λ = 1.5418 Å) radiation operated at 40 kV and 40 mA. Scanning was performed over the 2θ range of 2-20° at 5°/min. The N_2O, N_2, CO_2, CH_4, and O_2 adsorption/desorption isotherms were obtained using a Micromeritics ASAP 2460 surface area and pore size analyzer after the samples were activated (the temperature was 423 K and 523 K, vacuum was $1*10^{-10}$ bar) for 12 h. H_2O adsorption isotherms were obtained using an Autosorb-iQ Quantachrome (volumetric technique) at 298 K after the samples were activated for 12 h (the temperature was 423 K and 523 K, vacuum was $1*10^{-10}$ bar).

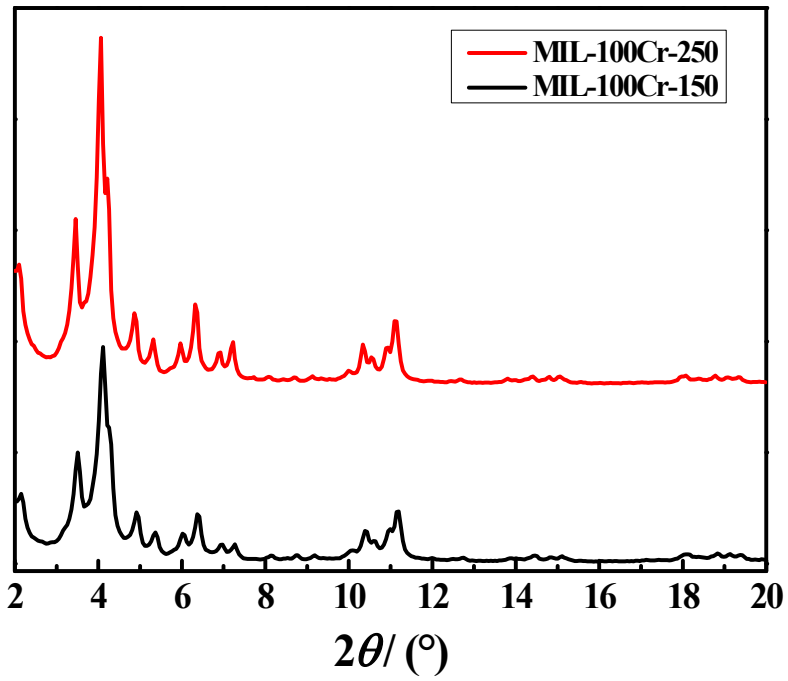

Fig. S1 XRD patterns of MIL-100Cr samples after activation at 423 K (MIL-100Cr-150) and 523 K (MIL-100Cr-250), respectively.

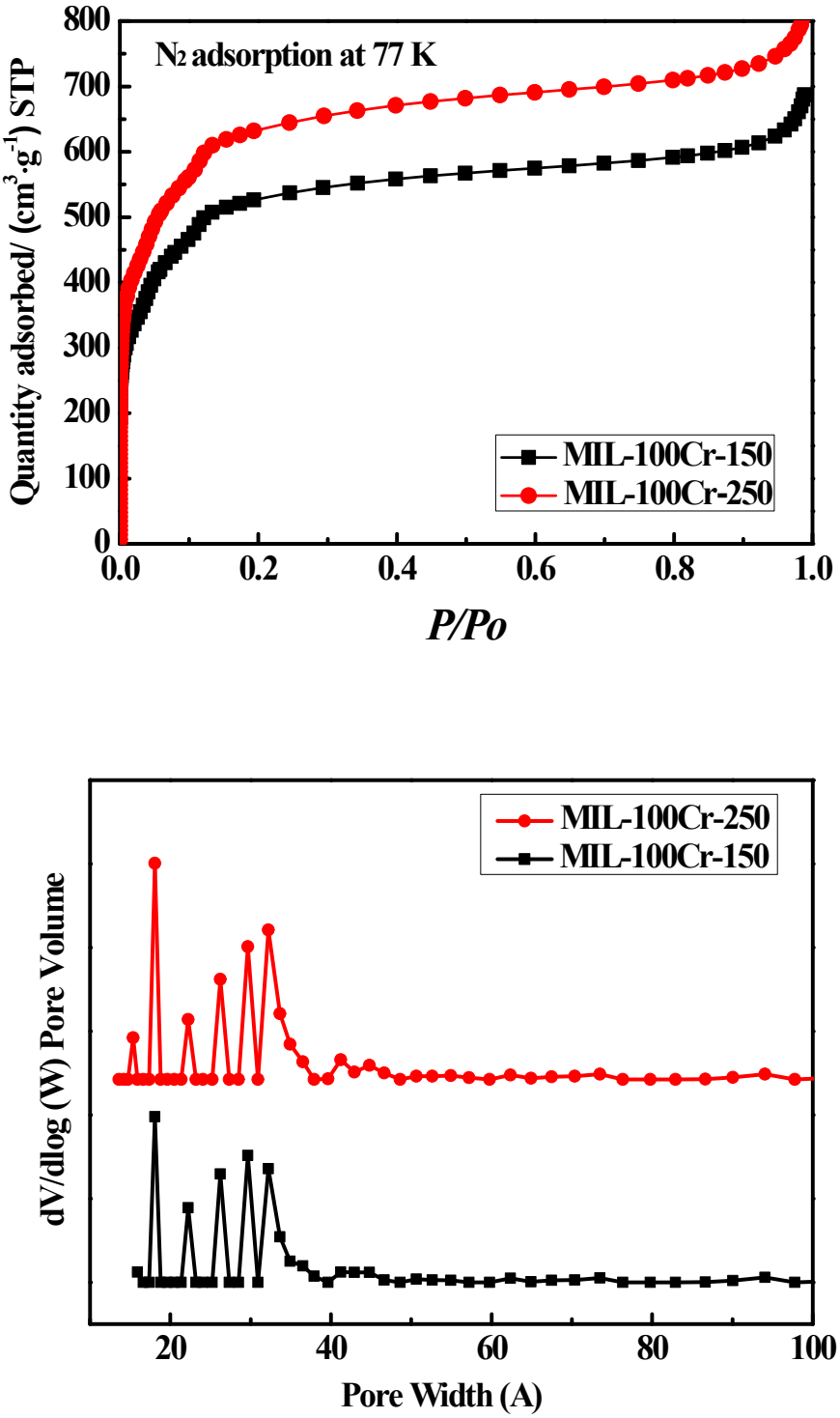

Fig. S2 N_2 adsorption and desorption isotherms of MIL-100Cr at 77 K and the pore size distribution calculated by the H-K method after activation at 423 K and 523 K.

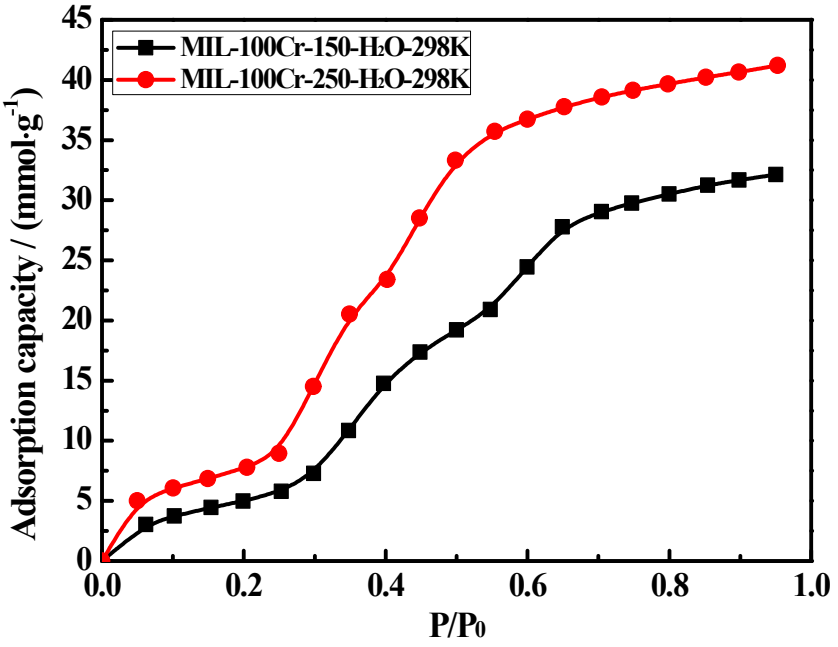

Fig. S3 Adsorption isotherms of H_2O on MIL-100Cr activated from 423 K and 523 K at 298 K

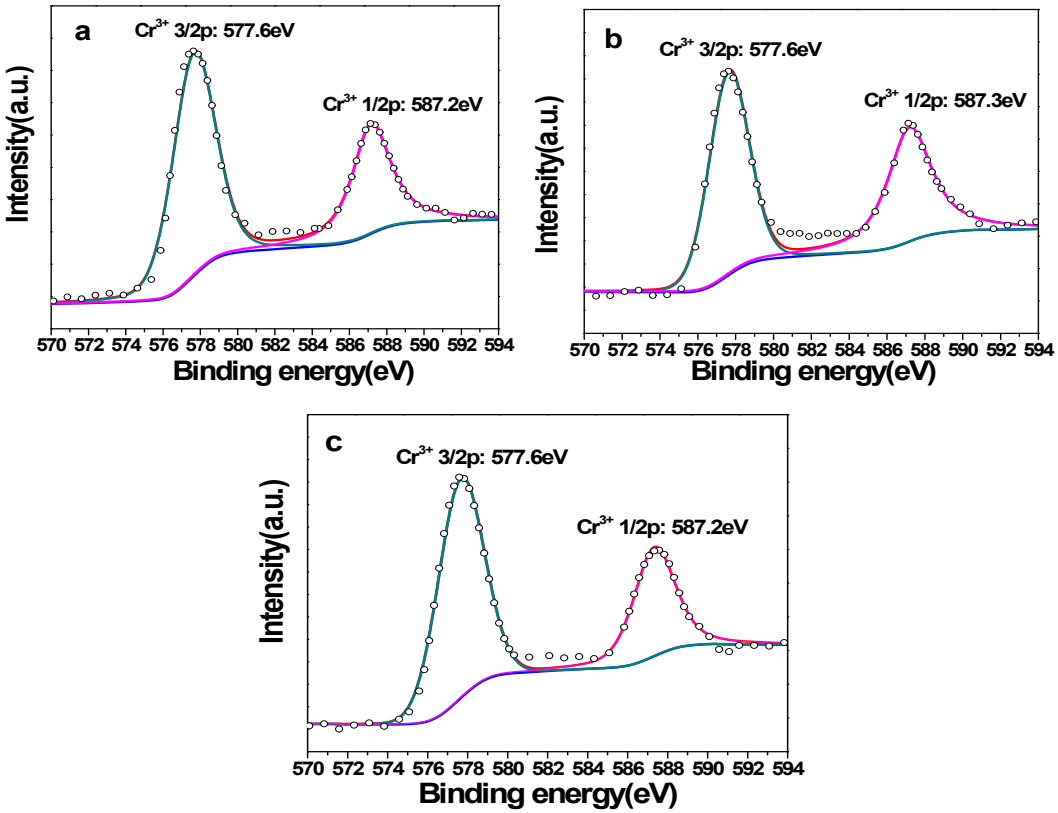

Fig. S4 High-resolution XPS spectra of Cr^{3+} 3/2p and Cr^{3+} 1/2p peaks for MIL-100Cr before (a) and after activation (b) at 523 K (MIL-100Cr-250), and also the N_2O adsorption on MIL-100Cr-250 (c).

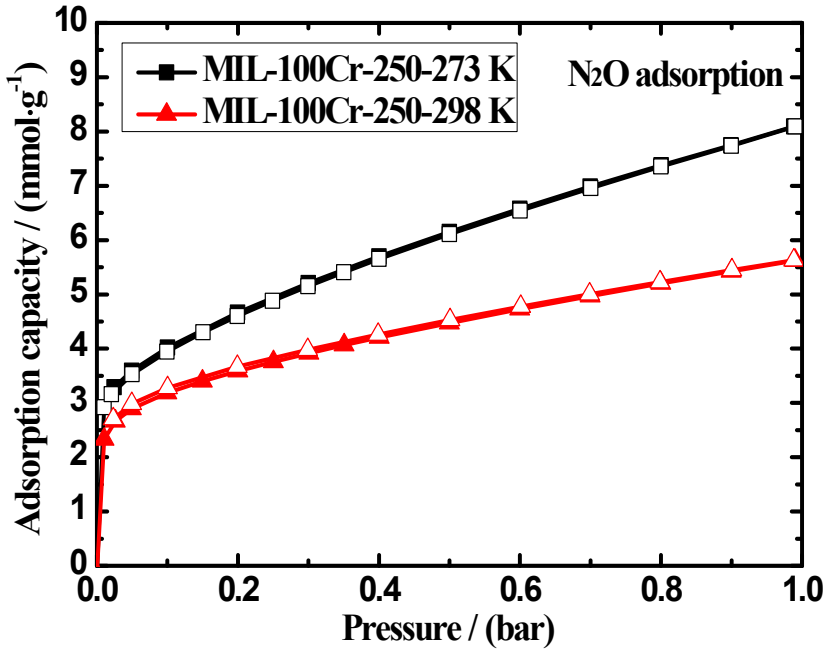

Fig. S5 Adsorption isotherms of N_2O on MIL-100Cr-250 at 298 K and 273 K.

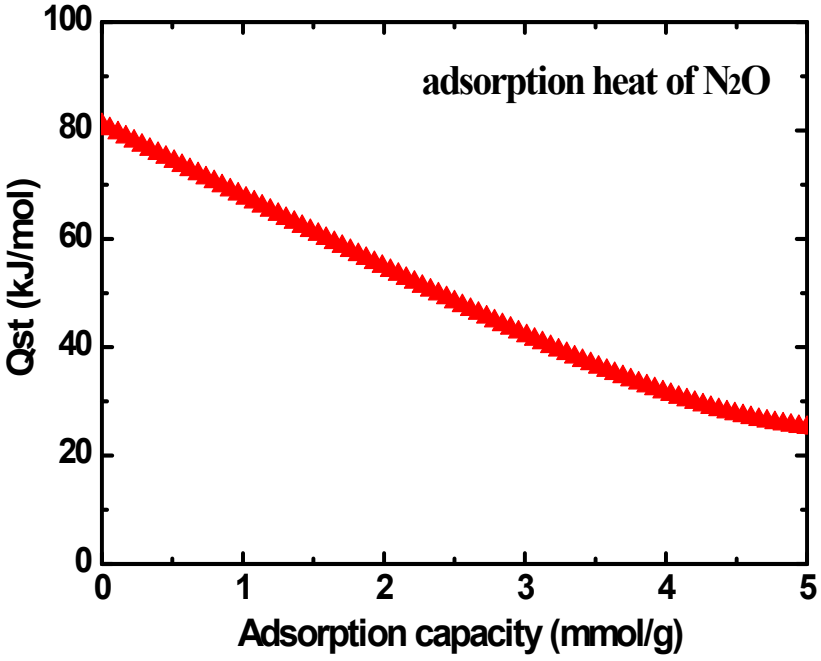

Fig. S6 Adsorption heat of N_2O on MIL-100Cr-250.

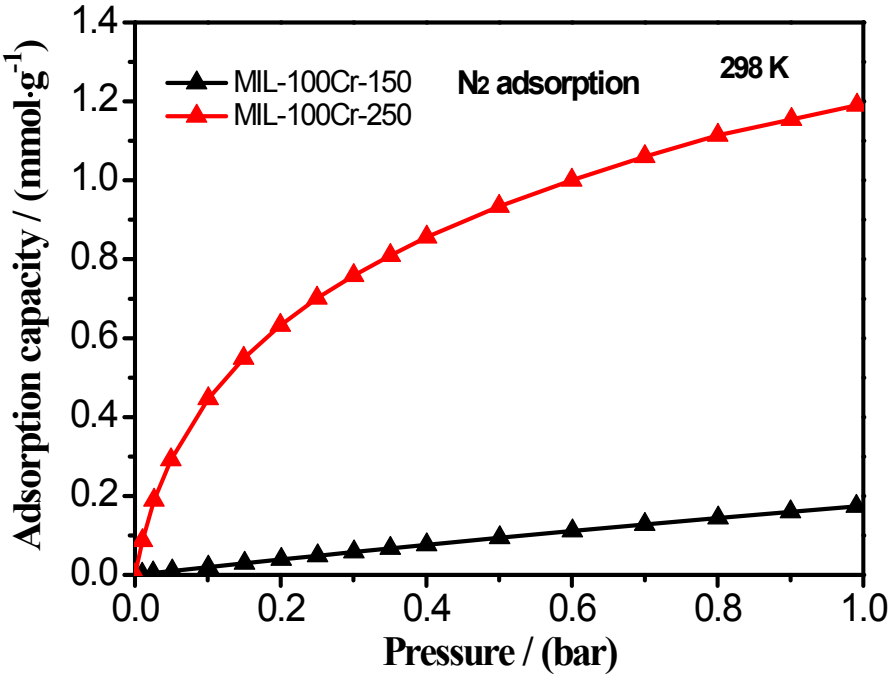

Fig. S7 Adsorption isotherms of N_2 on MIL-100Cr-150 and MIL-100Cr-250 at 298 K.

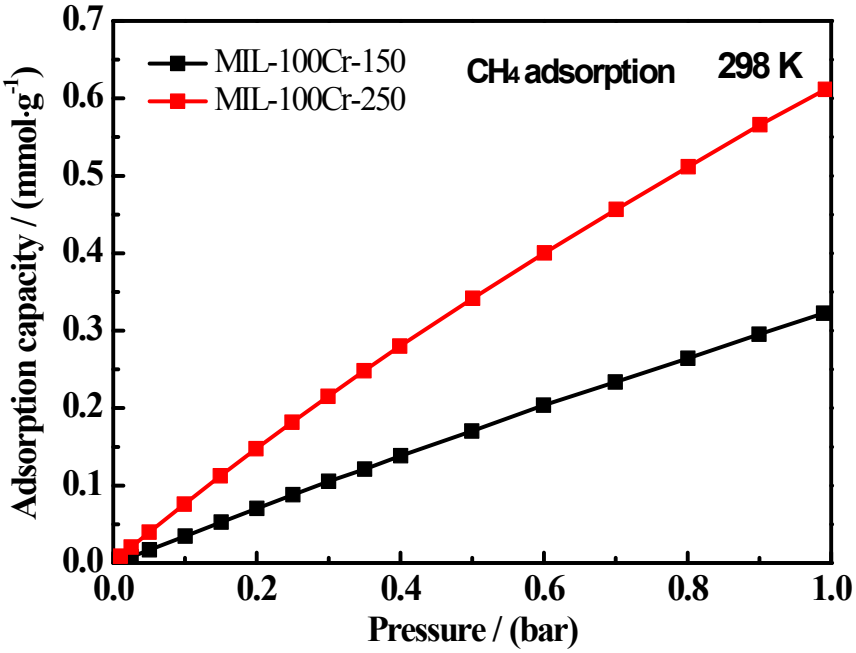

Fig. S8 Adsorption isotherms of CH_4 on MIL-100Cr-150 and MIL-100Cr-250 at 298 K.

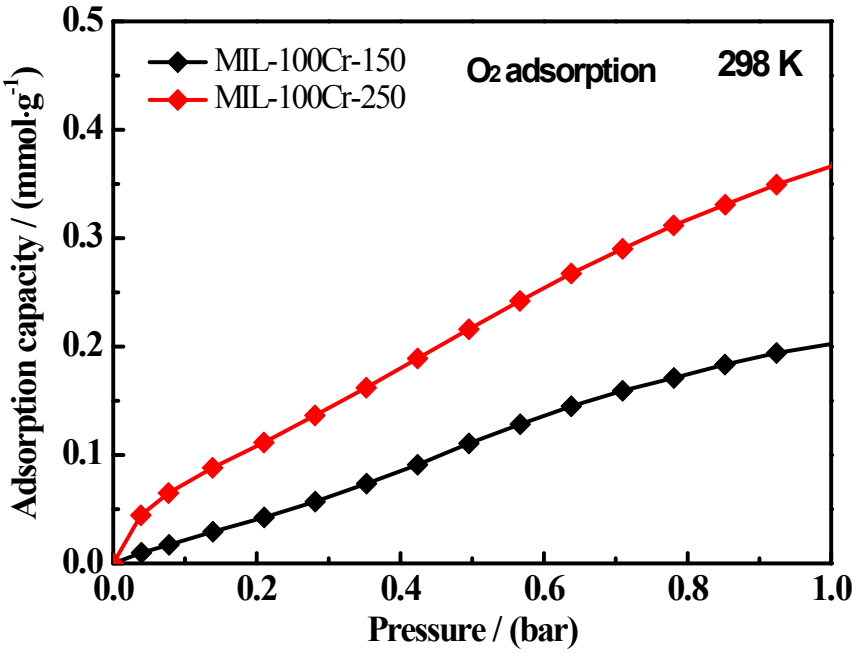

Fig. S9 Adsorption isotherms of O_2 on MIL-100Cr-150 and MIL-100Cr-250 at 298 K.

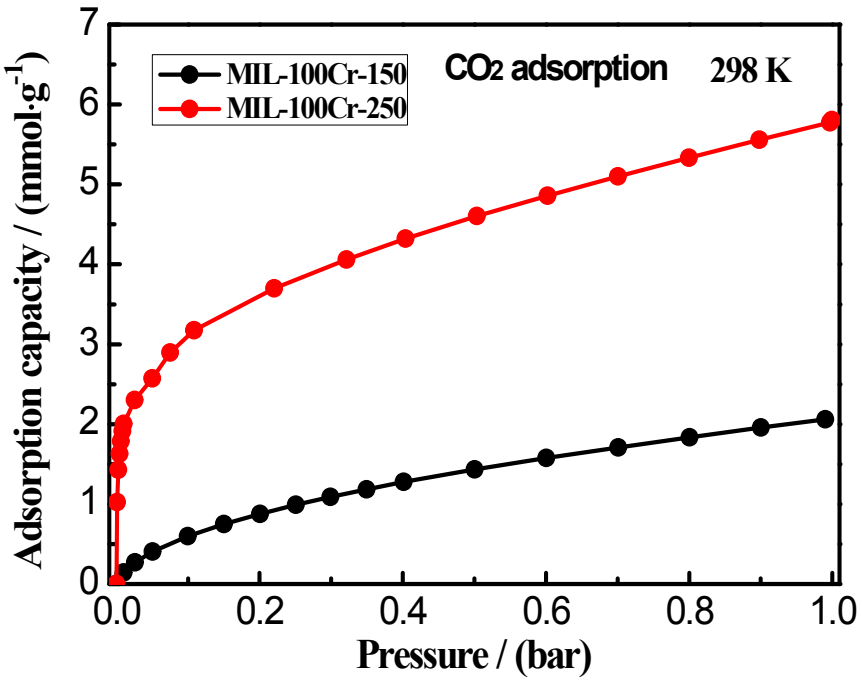

Fig. S10 Adsorption isotherms of CO_2 on MIL-100Cr-150 and MIL-100Cr-250 at 298 K.

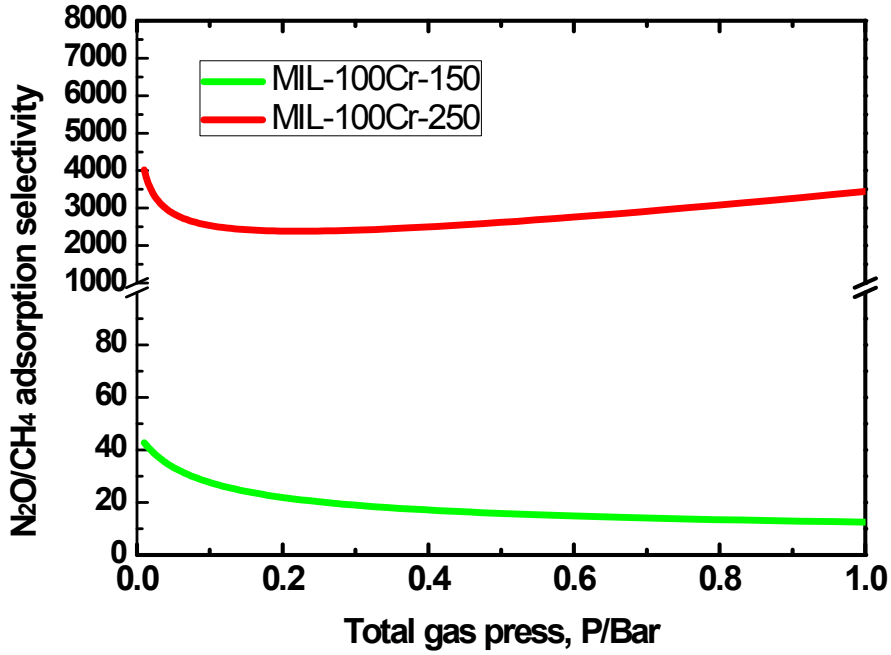

Fig. S11 Comparison of the ideal adsorbed solution theory (IAST) gas selectivity of 50/50 N_2O/CH_4 mixtures in MIL-100Cr-150 and MIL-100Cr-250 at 298 K.

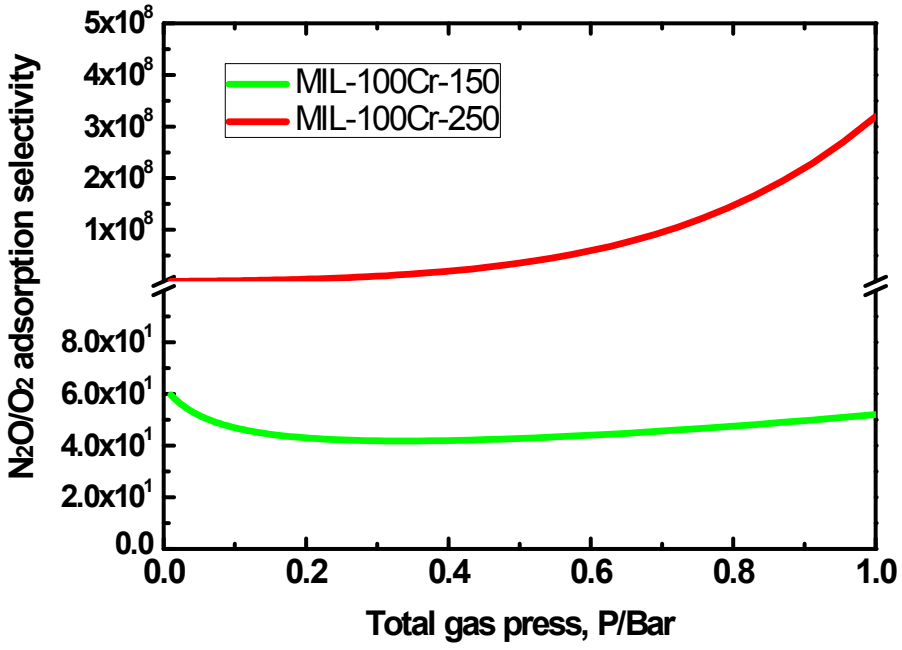

Fig. S12 Comparison of the ideal adsorbed solution theory (IAST) gas selectivity of 50/50 N_2O/O_2 mixtures in MIL-100Cr-150 and MIL-100Cr-250 at 298 K.

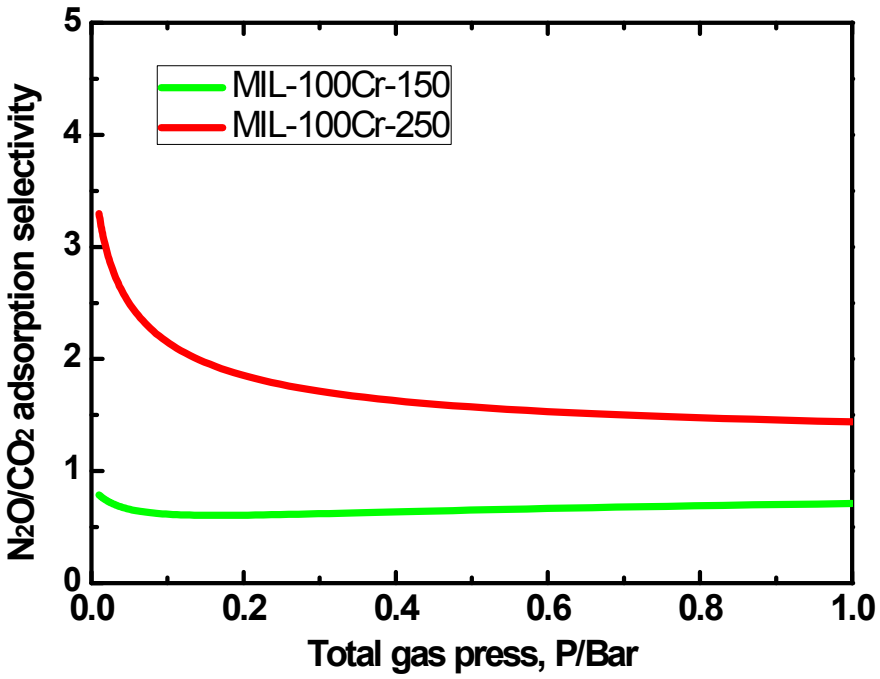

Fig. S13 Comparison of the ideal adsorbed solution theory (IAST) gas selectivity of 50/50 N_2O/CO_2 mixtures in MIL-100Cr-150 and MIL-100Cr-250 at 298 K.

2. Calculation

2.1. Density-functional theory calculations

Our First-principles density-functional theory (DFT) calculations were performed using the Quantum-Espresso package.[3] A semi-empirical addition of dispersive forces to conventional DFT was included in the calculation to account for van der Waals interactions.[4] We used Vanderbilt-type ultrasoft pseudopotentials and the generalized gradient approximation (GGA) with the Perdew-Burke-Ernzerhof (PBE) exchange correlation. Due to the large size of the MIL-100Cr unit cell and the large number of atoms, direct calculation on the MOF crystal structure is highly difficult. Therefore, we adopted a simplified cluster model (similar to the one used in ref. 5) to evaluate the gas binding. The Cr trimer metal center was cleaved from the periodic crystal structure of MIL-100Cr, and put in a 20×20×20 supercell. The carboxylate groups were terminated by H atoms, and the terminal F group on Cr was removed, which results in a net charge of +1 for the cluster. For this system, a cutoff energy of 544 eV and a 2×2×2 *k*-point mesh (generated using the Monkhosrt-Pack scheme) were found to be enough for total energy to converge within 0.01 meV/atom. The cluster

model (with "+1" charge) was first fully optimized with respect to atomic coordinates. The lowest-energy spin configuration for the three Cr ions is (+3, -3, +3), with the total spin value of the cluster being S=3. For gas adsorption, various possible binding configurations were considered and fully relaxed. The lowest-energy structures were identified as the optimal binding structures. To obtain the gas binding energies, a single gas molecule placed in a supercell with the same cell dimensions was also relaxed as a reference. The static binding energy (at T = 0 K) was calculated using: E_B = E(MOF) + E(gas) – E(MOF+gas).

2.2. Fitting of pure component isotherms

The unary isotherm data for N_2, O_2, and CH_4 in MIL-100Cr, measured at 298 K, were fitted with the single-site Langmuir model

$$q = q_{sat}\frac{bp}{1+bp} \tag{1}$$

The unary isotherm data for N_2O and CO_2 in MIL-100Cr, measured at 298 K, were fitted with the Dual-site Langmuir model

$$q = q_{A,sat}\frac{b_A p}{1+b_A p} + q_{B,sat}\frac{b_B p}{1+b_B p} \tag{2}$$

The isotherm fit parameters are provided in Table 1 to Table 5.

Table 1. Dual-site Langmuir fit parameters for N_2O in MIL-100Cr.

	$q_{A,sat}$ mol kg^{-1}	b_A Pa^{-1}	$q_{B,sat}$ mol kg^{-1}	b_B Pa^{-1}
MIL-100Cr 150	0.28	0.000475089	5.3	4.65563E-06
MIL-100Cr 250	2.1	0.024589204	5.7	1.61106E-05

Table 2. Dual-site Langmuir fit parameters for CO_2 in MIL-100Cr.

	$q_{A,sat}$ mol kg^{-1}	b_A Pa^{-1}	$q_{B,sat}$ mol kg^{-1}	b_B Pa^{-1}

MIL-100Cr 150	0.6	0.000268518	4.5	4.95596E-06
MIL-100Cr 250	2.4	0.004856163	5.8	1.34482E-05

Table 3. Single-site Langmuir fit parameters for N_2 in MIL-100Cr.

	q_{sat} mol kg^{-1}	b Pa^{-1}
MIL-100Cr 150	14	1.25717E-07
MIL-100Cr 250	1.4	4.38906E-05

Table 4. Single-site Langmuir fit parameters for CH_4 in MIL-100.

	q_{sat} mol kg^{-1}	b Pa^{-1}
MIL-100Cr 150	14	2.40748E-07
MIL-100Cr 250	3	2.59055E-06

Table 5. Single-site Langmuir fit parameters for O_2 in MIL-100Cr.

	q_{sat} mol kg^{-1}	b Pa^{-1}
MIL-100Cr 150	1	2.5E-06
MIL-100Cr 250	1	5.6E-06

2.3 Qst calculation

Qst is the adsorption isosteric enthalpy (−ΔH), which can be calculated as a function of loading using adsorption data at different temperatures via the Clausius−Clapeyron equation:

$$ln\frac{P_2}{P_1} = \frac{\Delta H}{R}(\frac{1}{T_1} - \frac{1}{T_2})$$

Where P is the pressure in bar, T is the temperature in K, R is the gas constant (8.314).

2.4. IAST calculations of adsorption selectivities, and uptake capacities

IAST calculations were performed to determine the separation selectivities of MIL-100Cr.

References

[1] P. Long, H. Wu, Q. Zhao, Y. Wang, J. Dong, J. Li, Solvent effect on the synthesis of MIL-96 (Cr) and MIL-100 (Cr). *Microporous and Mesoporous Materials***,** 142 (2) (2011) 489-493.

[2] J. Yang, Q. Zhao, J. Li, J. Dong, Synthesis of metal-organic framework MIL-101 in TMAOH-Cr(NO3)3-H2BDC-H2O and its hydrogen-storage behavior. *Microporous and Mesoporous Materials*, 130 (1-3) (2010) 174-179.

[3] P. Giannozzi, S. Baroni, and N. Bonini et al., *J. Phys. Condens. Matter.* 21 (2009), 395502.

[4] V. Barone, M. Casarin, D. Forrer, M. Pavone, M. Sambi, A. J. Vittadini, *Comput. Chem.* 30 (2009) 934.

[5] J. W. Yoon, H. Chang, S.-J. Lee, Y. K. Hwang, D.-Y. Hong, S.-K. Lee, J. S. Lee, S. Jang, T.-U. Yoon, K. Kwac, Y. Jung, R. S. Pillai, F. Faucher, A. Vimont, M. Daturi, G. Férey, C. Serre, G. Maurin, Y.-S. Bae and J.-S. Chang, *Nature Materials*, 16 (2016) 526.

[6] Y. Liu, J. Liu, M. Chang, C. Zheng, Effect of Functionalized Linker on CO2 Binding in Zeolitic Imidazolate Frameworks: Density Functional Theory Study, *The Journal of Physical Chemistry C* 116 (2012) 16985.

[7] B. Delley, Hardness conserving semilocal pseudopotentials, *Physical Review B* 66 (2002) 155125.

[8] P. Pulay, Improved SCF convergence acceleration, *Journal of Computational Chemistry* 3 (1982) 556.

[9] T.L. Hill, Statistical Mechanics of Adsorption. V. Thermodynamics and Heat of Adsorption. *J. Chem. Phys.* 17 (1949) 520-535.